



Single-Step Primary Amine Synthesis on Proton Sensitive Nanofilms to Overcome Its Debye Length Limitations

Yang, CM., Liu, HL., Ho, CC., Tsai, HF., & Bhalla, N. (2023). Single-Step Primary Amine Synthesis on Proton Sensitive Nanofilms to Overcome Its Debye Length Limitations. *Advanced Materials Interfaces*, 10(21), 1-9. [2300080]. <https://doi.org/10.1002/admi.202300080>

[Link to publication record in Ulster University Research Portal](#)

Published in:

Advanced Materials Interfaces

Publication Status:

Published (in print/issue): 26/07/2023

DOI:

[10.1002/admi.202300080](https://doi.org/10.1002/admi.202300080)

Document Version

Publisher's PDF, also known as Version of record

General rights

Copyright for the publications made accessible via Ulster University's Research Portal is retained by the author(s) and / or other copyright owners and it is a condition of accessing these publications that users recognise and abide by the legal requirements associated with these rights.

Take down policy

The Research Portal is Ulster University's institutional repository that provides access to Ulster's research outputs. Every effort has been made to ensure that content in the Research Portal does not infringe any person's rights, or applicable UK laws. If you discover content in the Research Portal that you believe breaches copyright or violates any law, please contact pure-support@ulster.ac.uk.

Single-Step Primary Amine Synthesis on Proton Sensitive Nanofilms to Overcome Its Debye Length Limitations

Chia-Ming Yang, Hui-Ling Liu, Chih-Ching Ho, Hsieh-Fu Tsai, and Nikhil Bhalla*

The Debye length is a measure of the distance over which the electric field of a charged particle decays in an electrolyte solution. If the binding of the analyte to the surface of the transducer is too far away from the surface, the electric field to the analyte may decay over a distance greater than the Debye length thereby reducing the sensitivity of the measurement. In this context, this study has developed a simple one-step protein immobilization strategy to covalently attach proteins on the sensor surface. Our binding strategy, which uses hydrogen peroxide (H_2O_2) ensures that the analyte is attached as close as possible to the transducer surface. This study evaluates our findings by comparing our strategy with silane chemistry and elucidating the Debye length effects with colorimetric assays and field effect devices. Additionally, as a case study, we also evaluated the performance of our methodology for the detection of glucose oxidation by a field effect device. Overall, the developed immobilization strategy avoids the effects of the Debye length and improves the performance of the biosensor.

1. Introduction

Handshake of the analyte with the transducer triggers a sensor response, which determines the presence and concentration of the analyte. This handshake of the analyte with the surface of the transducer should be as close as possible in order to avoid the effects of the Debye length. On the other hand, the formation of primary amines on solid surfaces is useful for attaching proteins that form biorecognition layers in bio/chemical sensors.^[1] The most common materials used for transducer elements within the bio/chemical sensors are either gold^[2] or silicon^[3] based materials, where covalent attachment of proteins is achieved by thiol chemistry or

C.-M. Yang, H.-L. Liu, C.-C. Ho
Department of Electronic Engineering
Chang Gung University
Taoyuan City 33302, Taiwan

C.-M. Yang
Institute of Electro-Optical Engineering
Chang Gung University
Taoyuan City 33302, Taiwan

C.-M. Yang
Biosensor Group
Biomedical Engineering Research Center
Chang Gung University
Taoyuan City 33302, Taiwan

C.-M. Yang
Department of General Surgery
Chang Gung Memorial Hospital at Linkou
Taoyuan City 33302, Taiwan

C.-M. Yang
Department of Neurosurgery
Chang Gung Memorial Hospital at Linkou
Taoyuan City 33302, Taiwan


C.-M. Yang
Department of Materials Engineering
Ming Chi University of Technology
New Taipei City 23652, Taiwan

H.-F. Tsai
Department of Biomedical Engineering
Chang Gung University
Taoyuan City 33302, Taiwan

H.-F. Tsai
Department of Neurosurgery
Chang Gung Memorial Hospital
Keelung, Keelung City 204, Taiwan

N. Bhalla
Nanotechnology and Integrated Bioengineering Centre (NIBEC)
School of Engineering
Ulster University
York Street, Belfast, Northern Ireland BT15 1ED, UK
E-mail: n.bhalla@ulster.ac.uk

N. Bhalla
Healthcare Technology Hub
Ulster University
York Street, Belfast, Northern Ireland BT15 1ED, UK

 The ORCID identification number(s) for the author(s) of this article can be found under <https://doi.org/10.1002/admi.202300080>

© 2023 The Authors. Advanced Materials Interfaces published by Wiley-VCH GmbH. This is an open access article under the terms of the Creative Commons Attribution License, which permits use, distribution and reproduction in any medium, provided the original work is properly cited.

DOI: 10.1002/admi.202300080

silane chemistry, respectively.^[4] The thiol or silane adlayer, even with a monolayer thickness on the transducer surface, creates a distance (e.g., few nanometers) between the transducer surface and the analyte, leading to a reduced interaction between the analyte and the transducer.^[5,6] This is one of the fundamental limits of the sensor-analyte interaction, which has hindered the use of several electrochemical and optical transducers to maximize their potential for ultrasensitive biomolecule detection.^[7,8] For instance, in the case of proton sensitive nanofilms-such as silicon nitride (Si_3N_4), tantalum pentoxide (Ta_2O_5), silicon dioxide (SiO_2), or aluminum oxide (Al_2O_3), commonly used as top layer of Ion Sensitive Field Effect Devices (ISFEDs),^[9–11] one must ensure that the sensor-analyte handshake takes place within the Debye length. Note that the term ISFED here includes both the Ion Sensitive Field Effect Transistors (ISFETs) and the Electrolyte Insulator Semiconductor (EIS) structures.

Debye length is the distance, away from the transducer surface, within which the moving charge carriers in the solution screen out the applied electric field present on the transducer surface.^[12] Essentially, any minute charge changes which take place in the solution outside the Debye length are difficult to detect by the aforementioned proton/pH sensitive transducers.^[13,14] On the other hand, the surface chemistry used to build the biorecognition layers often yield biomolecular charge change signatures at distances beyond the Debye length, thereby reducing the sensitivity of the transducer.^[15,16] Therefore, for such sensors, biomolecular interaction should comply with the prerequisite for distances-where an electric field caused by redistributed charged biomolecules exists within the Debye length of the given solution.

To overcome these issues in ISFEDs, several innovative approaches have been developed, such as the stem loop structures, which cause conformational changes in the biomolecule upon ligand binding,^[17] those that involve use of novel semiconductors with specific carrier distribution,^[18] with use of polymer enhancers embedded inside the ISFEDs structure,^[19] by improving material morphology,^[20] with changes in the salt/ion concentration (i.e., changes in the ionic strength) of buffer and by reducing the distance of analyte to the transducer surface.^[21] While each of these strategies is unique and has its own advantage, there are a few loopholes associated with these methods. For example, change in the salt/ion concentration of the buffer may increase the Debye length at the cost of changes in the conformational properties of the capture molecule, leading to a reduced sensitivity of the biorecognition layer toward the analyte. This is because the biomolecules need certain buffer conditions to maintain their osmolarity, which is necessary for effective binding.^[22] Other methods involving the use of polymers and special substrate, such as crumpled graphene, have their own challenges mainly associated with nanoscale fabrication of the material, optimization of the process for large scale development of ISFED sensor and device degradation at high/low temperatures.

Within this context, we have developed a simple method that uses directly synthesized primary amines to covalently attach proteins on the Si_3N_4 surface, see **Figure 1** for more details. This is in contrast with the conventional route of incorporating silane monolayers on the Si_3N_4 based substrates. Briefly, we incubate the Si_3N_4 surfaces in H_2O_2 which leads to the creation of primary amine groups ($-\text{NH}_2$) as Si_3N_4 degrades into oxygen (O_2)

and water (H_2O) via disproportionation reaction. The decomposition of H_2O_2 to form water H_2O and O_2 is well-known as a disproportionation reaction i.e., it is simultaneously oxidized and reduced, giving two different products.^[23] This is because the oxygen element of the peroxide compound is in -1 oxidation state and it is converted to 0 oxidation state in oxygen (H_2O oxidized) and -2 oxidation state (H_2O reduced). It should be noted this decomposition of H_2O_2 is performed in ambient white light of the room, without any catalysts. The use of several nanocatalysts suggested in the literature for H_2O_2 decomposition is primarily to speed with reaction kinetics of the natural decomposition process.^[24,25] The water then reacts with Si_3N_4 surfaces to yield primary amines. These amines are further used for attaching proteins on the Si_3N_4 surfaces. Finally, the performance of the sensor was also compared with most common silanization procedures, which use 3-Aminopropyl-triethoxysilane (APTES) and 3-Glycidyloxypropyl-trimethoxysilane (GOPTS). The enhanced sensing performance achieved using our new method was evaluated using capacitance-voltage characterization of the ISFED which revealed higher sensitivity of H_2O_2 based immobilization strategy due to reduced Debye length effects. Overall our method was found to be more reproducible, user-friendly as it avoided silane preparation steps and exposure to its fumes.

2. Results and Discussion

2.1. Surface Treatment and Bioassays

The Si_3N_4 surface was exposed to H_2O_2 by drop casting method. Essentially, a drop of 8.25% H_2O_2 , covering complete surface of the Si_3N_4 (around 150 μl for a substrate size of 1 cm x 1 cm) was placed on the top surface of the silicon nitride for 3 h. In parallel, we also incubated the substrate in 5% APTES in mixed acetone for 6 h. Upon comparison of silicon nitride surface state with Fourier Transform Infrared Spectroscopy (FTIR) for the aforementioned APTES and H_2O_2 treatments, we observed no significant differences in transmission characteristics between the two treated surfaces, see **Figure 2a**. The surfaces were then exposed to glutaraldehyde (GA), 15% in water for 3h. Once again, we observed no significant differences between APTES and H_2O_2 treated surfaces after GA immobilization, see **Figure 2b**. This confirmed that H_2O_2 treatment creates chemical modification similar to APTES treatment i.e., the formation of primary amines that also readily attached (covalently) with the aldehyde groups of GA. Furthermore, we compared the surface of the silicon nitride before and after the treatment of H_2O_2 that revealed clusters of small peaks (marked with circles, **Figure 2c**) between 3000–4000 cm^{-1} that are attributed to the formation of primary amine groups on its surface.^[26,27] The H_2O_2 treated surface (after GA immobilization) was exposed to an anti-protein A antibody conjugated with horseradish peroxidase (HRP), which facilitates colorimetric detection via oxidation of 3,3',5,5'-Tetramethylbenzidine (TMB). The contact angle measurements, see **Figure 2d** revealed similar surface properties for all steps involved in the Protein A immobilization using H_2O_2 treatment method compared to Protein A immobilization using the APTES treatment.

We also measured the color change of the TMB, using absorbance spectroscopy as shown in **Figure 3**. For absorbance

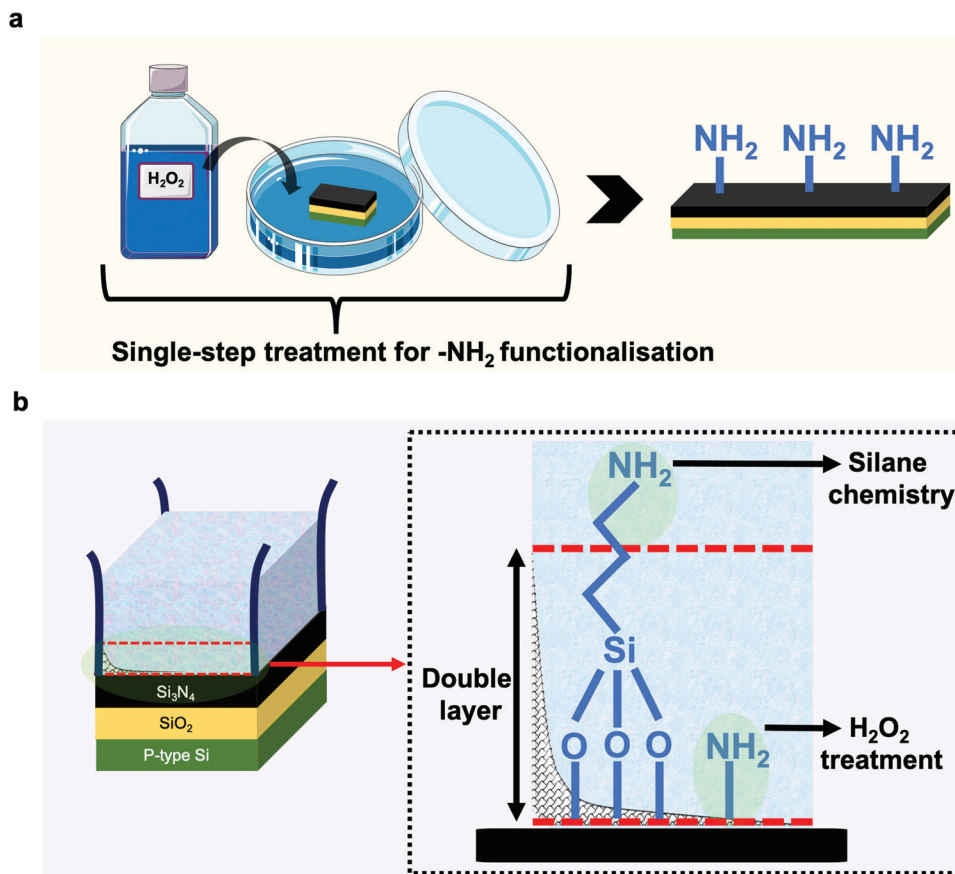


Figure 1. Schematic of surface treatment concept: a) shows a single step H_2O_2 treatment on Si_3N_4 surface leading to creation of primary amines on the sensor surface when dipped inside a solution consisting H_2O_2 in a petri dish. Note that the petri dish is kept closed during the incubation of the sensors in H_2O_2 ; b) shows electrolyte-insulator-semiconductor surface used to elucidate Debye length effects using capacitance-voltage characteristics for H_2O_2 treated surfaces while comparing it with silane chemistry using APTES.

comparison, apart from APTES comparison we also compared immobilization of Protein A with (3-Glycidioxypropyl)trimethoxysilane (GOPTS). Figure 3a shows the TMB absorbance from treated (treated with APTES, GOPTS and H_2O_2) substrates. Clearly the absorbance from H_2O_2 was found to be the highest among the three treatments, suggesting that more Protein A was present on the surface. Control reactions were also performed by blocking the aldehyde group of GA with 0.2 M ethanolamine in case of APTES and H_2O_2 treatments, and blocking GOPTS with 20% ethanol, see Figure 3b ($n \geq 6$). In Figure 3c, we plot the total area under the curves of treated and control experiment replicates to show the absorbance values. We also perform two-way ANOVA Šidák's multiple comparisons test to reveal statistical differences between the three sets of treatments. The treatment of H_2O_2 showed significantly higher absorbance (confidence interval of 95%; P value < 0.001). We also extended our analysis to compare the absorbance peaks of treated and control experiment replicates ($n \geq 6$), in Figure 3d, e, at 370 and 650 nm, respectively. The comparison clearly shows higher absorbance from the H_2O_2 treatment, even for the control experiments. Therefore, we compared the ratio between the peaks of treated and control experiments, which indicate that the absorbance at 370 nm in H_2O_2 treatment is the highest among the three sets of experiments, see

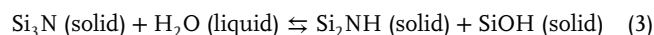
Figure 3f. Motivated by our finding we changed the concentration and/or time of incubation of H_2O_2 to optimize the amount of protein attachment on the surface. We find that the H_2O_2 (8.25% aq.) exposure for 3 h allowed maximum amount of anti-protein A to attach on the surface of the Si_3N_4 , see Figure 3g for comparison of absorbance with other experimental conditions.

2.2. Chemical Reaction

When H_2O_2 comes in contact with the Si_3N_4 substrate, it decomposes via disproportionation reaction as follows:



The water formed after reduction of H_2O_2 reacts with the Si_3N_4 , which is the highest species present on the surface of the Si_3N_4 , yielding SiOH and SiNH_2 sites according to the following reactions:^[28]



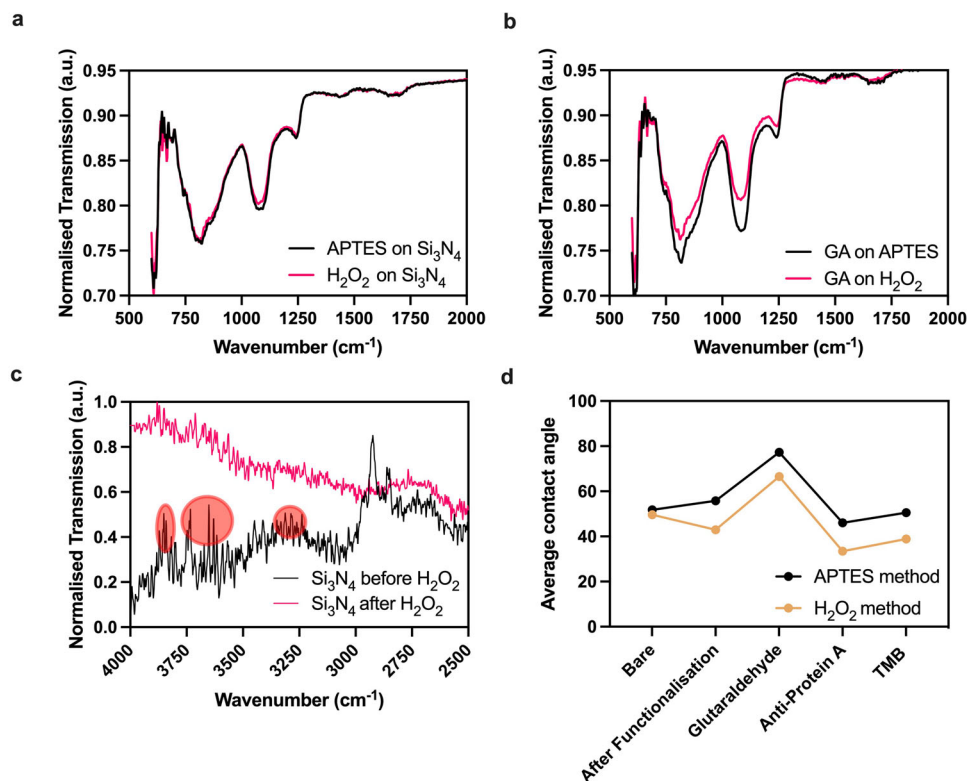
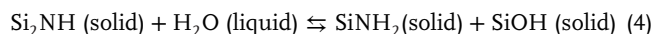


Figure 2. Si₃N₄ surface characterization: a) FTIR of APTES and H₂O₂ treated Si₃N₄ surface; b) FTIR of addition of GA on APTES and H₂O₂ treated Si₃N₄ surface; c) FTIR of Si₃N₄ surface before and after treatment with H₂O₂; d) Average ($n = 3$ measurements) contact change of the Si₃N₄ surface upon treatment with APTES/H₂O₂ (referred to as after functionalization), GA, Anti-protein A and TMB dye.



Since the reaction is reversible, prolonging the reaction for more than 3 h will lead to formation of water and tertiary amines. This is primarily why we see less amount of Protein A attachment on our surface for the experiment where H₂O₂ incubation was performed for 24 h.

2.3. Debye Length Effect

In the field-effect sensing, the basic characteristic of a device should be a concentration-relative response to ion concentrations on the surface, which is influenced by the debye-length effect.^[29–31] The Si₃N₄/SiO₂/Si structure used in this work is a conventional ISFED often used for pH sensing applications. As debye length effect is strongly dependent on the ionic strength, our Si₃N₄/SiO₂/Si ISFED was exposed to different concentrations (150 mM, 15 mM, and 1.5 mM) of PBS solutions. One peculiar feature of such structures is the capacitance–voltage (C – V) response, where the capacitance is strongly dependent on the frequency, which is further dependent on the relative charging ability of the ions to form an electrical double layer.^[32] We measured the C – V curves of Si₃N₄/SiO₂/Si in aforementioned concentrations of PBS solution as shown in Figure 4a–c.

In Figure 4, a typical behavior with accumulation, depletions, and inversion regions from negative to positive gate bias voltage can be observed with the change in capacitance.^[33,34] With

changes in frequency, the capacitance of the accumulation and inversion regions decreases, which is similar to the reports in literature.^[35,36] It can also be clearly observed that with the use of low PBS concentration (e.g., 0.01X PBS) there is a more decrease in the capacitance (accumulation, depletion, and inversion) as the frequency is increased, compared to those measured in high PBS concentration (e.g., 1x PBS).

We discuss this frequency dependence of ISFED structure in the context of the immobilisation enabled by H₂O₂ treatment. As shown in Figure 4d–f, there are minute changes in the capacitance in the region of positive gate bias voltage (the curve is mostly flat after 0 V) at all frequencies. This can be attributed to the charges of the immobilized surface chemistry (including antibodies) that form the inversion layer. It should be noted that no change in the trend of capacitance is observed in the depletion layer when compared to C – V characteristics without functionalization (i.e., comparison of Figure 4a–c with Figure 4d–f). However, at frequencies higher than 5 kHz, the capacitance of accumulation region of the surface functionalized samples, Figure 4d–f, at 0.01X PBS shows a larger decrease in its capacitance when compared to the C – V characteristics without functionalization Figure 4a–c. This frequency dependent capacitance, which decreases in low ionic strength electrolyte is ascribed to the debye length effect. We explain this with a simple equation, Equation (5), describing capacitance of a parallel plate capacitor:

$$C = \epsilon_0 \epsilon_m \frac{A}{d} \quad (5)$$

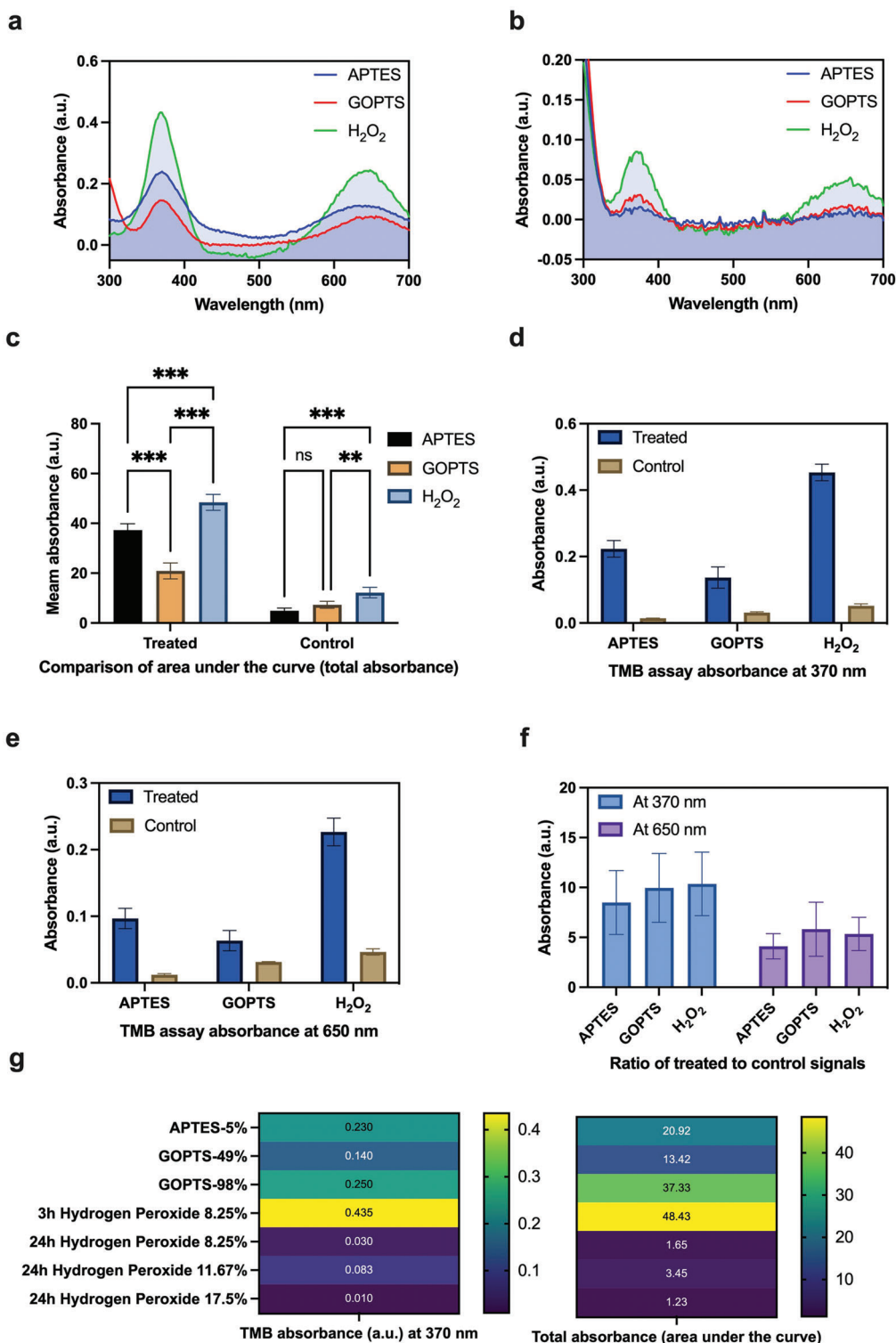


Figure 3. Surfaces functionalization comparison: a) Wavelength versus absorbance characteristics of TMB dye when reacted with HRP-linked proteins on the APTES, GOPTS, and H_2O_2 modified Si_3N_4 surfaces. We call refer to this experiment as 'treated'; b) Wavelength versus absorbance characteristics of TMB dye when reacted with non-specifically absorbed HRP-linked proteins on the APTES, GOPTS, and H_2O_2 modified surfaces. Note that here the sensor surface was blocked with ethanolamine and in an ideal case, no peaks corresponding to TMB dye should be observed. We call refer to this experiment as 'control'; c) Total absorbance comparison (area under the curves) for treated and control experiments. d) Comparison of TMB assay at absorbance 370 nm performed for treated and control; e) Comparison of TMB assay at absorbance 650 nm performed for treated and control; f) Ratio of treated to control signals from TMB assay; g) Heat plot showing various conditions used for H_2O_2 , APTES and GOPTS treatments.

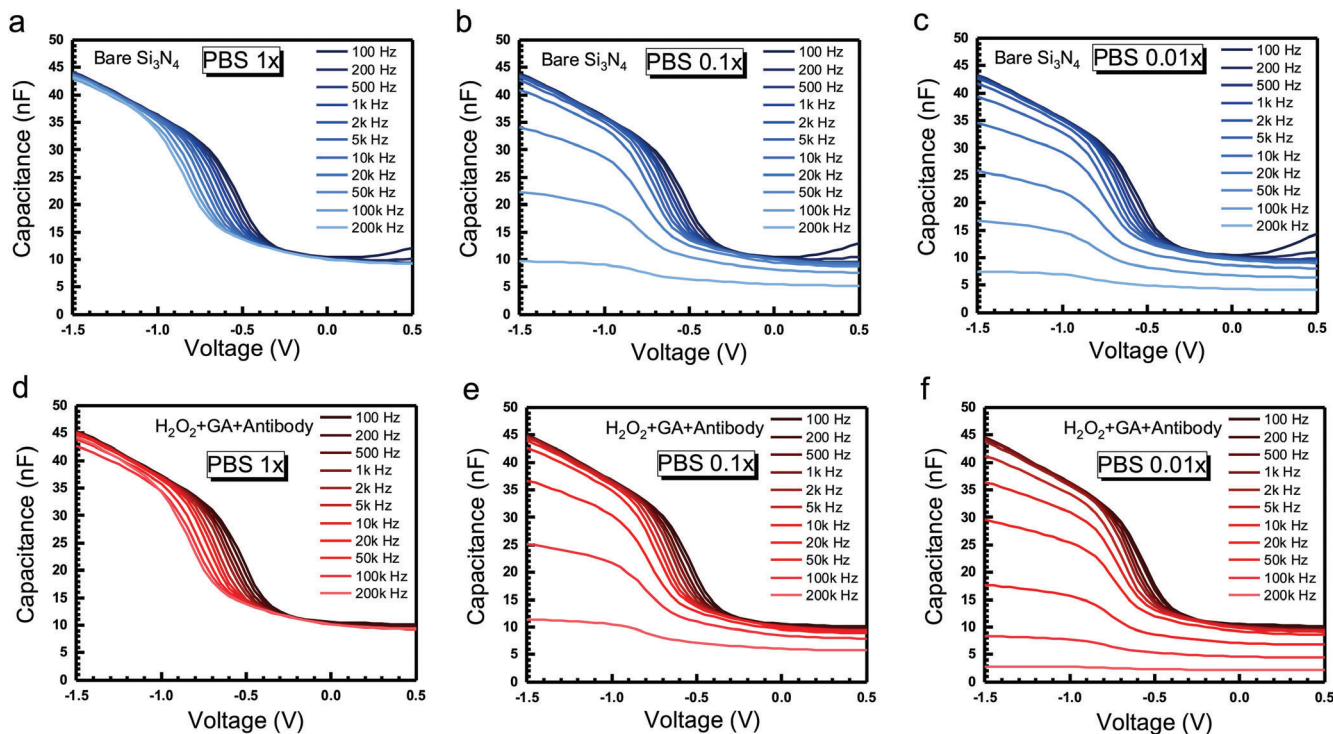


Figure 4. Capacitance–Voltage (C – V) characterization: a) shows curves of $\text{Si}_3\text{N}_4/\text{SiO}_2/\text{Si}$ ISFED measured at different frequencies in 1X; b) at 0.1X and c) at 0.01X PBS buffer solution. d) shows C – V curves of $\text{Si}_3\text{N}_4/\text{SiO}_2/\text{Si}$ after the modification of H_2O_2 , GA, and antibody, e) at 0.1X and f) at 0.01X PBS buffer solution. Note that 1X is 150 mM, 0.1X is 15 mM and 0.0X is 1.5 mM concentrations.

here, C is the accumulation capacitance, ϵ_0 is the permittivity in vacuum, ϵ_m is the relative permittivity, A represents Area and d is the distance between the two plates of the capacitor. It should be noted that the accumulation capacitance of EIS structure is mainly determined by the series of insulator and electrical double layer. Since the thickness of insulator is fixed, the effective capacitance is dominated by the electrical double layer formation in different electrolytes. Additionally, the thickness of electrical double layer is highly relative to Debye length ($1/\kappa$) as shown by Dukhin et al.,^[37] which is relative to the conductivity, permittivity, and diffusion coefficient of solution according to Equation (6).

$$\kappa^2 = \frac{K_m}{\epsilon_0 \epsilon_m D_{eff}} \quad (6)$$

where K_m and D_{eff} is the conductivity and effective diffusion coefficient of the solution. Therefore, Debye length ($1/\kappa$) is inversely proportional to the square root of the ion strength and corresponding conductivity. This means that at higher ion strength, higher permittivity, and the higher capacitance can be observed, as also observed by Liu et al.^[38] In their work, the capacitance and permittivity is decreased with frequency, which is attributed to the Debye relaxation and therefore in the low ion strength electrolyte, a large Debye length can be obtained for a better detection of biomarker. In similar lines, the more decrease in accumulation capacitance at high frequency of H_2O_2 treated

surface is associated with a similar effect of low ion strength buffer.

We plot the effect of H_2O_2 treated and APTES treated surfaces, capacitance at -1.5 V versus frequency curve, and use this as a new index to evaluate the ionic strength effect as shown in Figure 5a,b, respectively. It is clearly seen that at higher frequency, the capacitance of accumulation region decreases, especially at low PBS concentration. Capacitance measured at 1X PBS solution are almost not impacted by frequency. Therefore, only the capacitance difference between bare and surface with antibody attached with different functionalizations (H_2O_2 or APTES) at 0.1X and 0.01X PBS solution is calculated to plot with the corresponding frequency as shown in Figure 5c. A large capacitance difference can be seen for the group measured at 0.01X PBS solution and with H_2O_2 treatment compared to the group measured at 0.1X PBS solution and with APTES treatment, respectively. This behavior is well-matched to the hypothesis of less debye length effects, yielding better sensing by a short linker from H_2O_2 . This is because large changes in the accumulation capacitance in H_2O_2 treatment compared to APTES treatment, can be ascribed to the presence of more charged species within the debye length (as attached molecules are closer to the electrode surface in H_2O_2 treatment). As a result, there is more screening of charge by the mobile carriers of the electrode, ISFED structure in this our study, leading to higher amounts of signal change in response to stimulus of biomolecule attachment on the electrode. This aspect is crucial in enhancing the sensitivity of the ISFED toward the target as

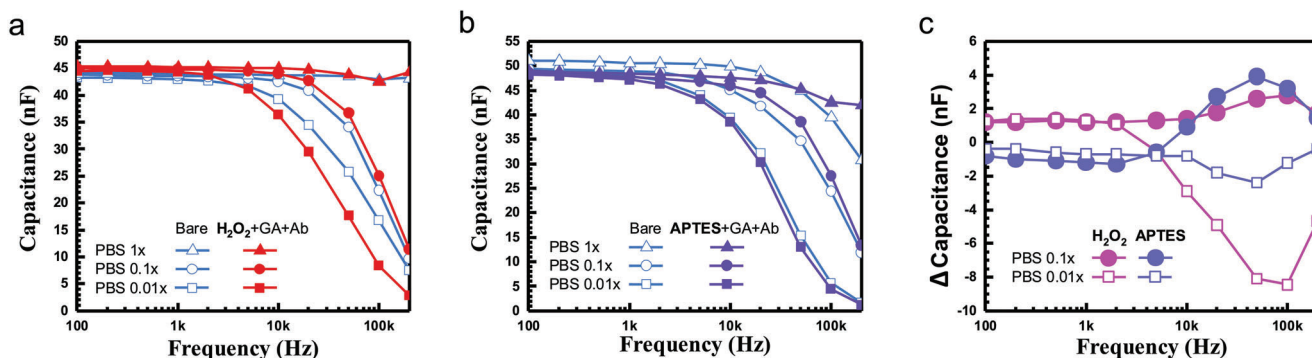


Figure 5. Capacitance versus frequency analysis: The capacitance at -1.5 V versus frequencies ($C-F$) curves measured in different concentration of PBS buffer solution for ISFED Device a) without and with modification of H_2O_2 , GA, and alpha-synuclein antibody; b) with and without modification of APTES, GA, and alpha-synuclein antibody and c) shows the capacitance difference between bare surface and after antibody immobilization step, at the same frequency, between H_2O_2 and APTES surface treatments.

demonstrated by our comparative study using various immobilization methods.

2.4. Detection of Glucose Oxidation Activity

Although we demonstrate superior binding of proteins in the sensor surface modified with H_2O_2 for colorimetric assays using Protein A, we here show the effect of reduced Debye length on the detection of glucose oxidation by the ISFED device. We first measure the pH response of the $Si_3N_4/SiO_2/Si$ structure using

pH 4, 7, and 10. The mean pH sensitivity of bare Si_3N_4 , H_2O_2 treated and APTES treated surfaces were found to be 48.3, 46.8, and 42.1 mV/pH respectively, see **Figure 6a**. There is no significant difference between the between pH sensitivity of bare Si_3N_4 and the H_2O_2 treated surfaces. In contrast, there is a significant difference between pH sensitivities of APTES treated surfaces compared to bare Si_3N_4 and H_2O_2 treated surfaces. It should be noted that this statistical analysis is performed using Tukey's multiple comparisons test with alpha value = 0.05. This is attributed to the combinatorial effect of less $-OH$ sites available on the Si_3N_4 surface after attachment of the APTES and

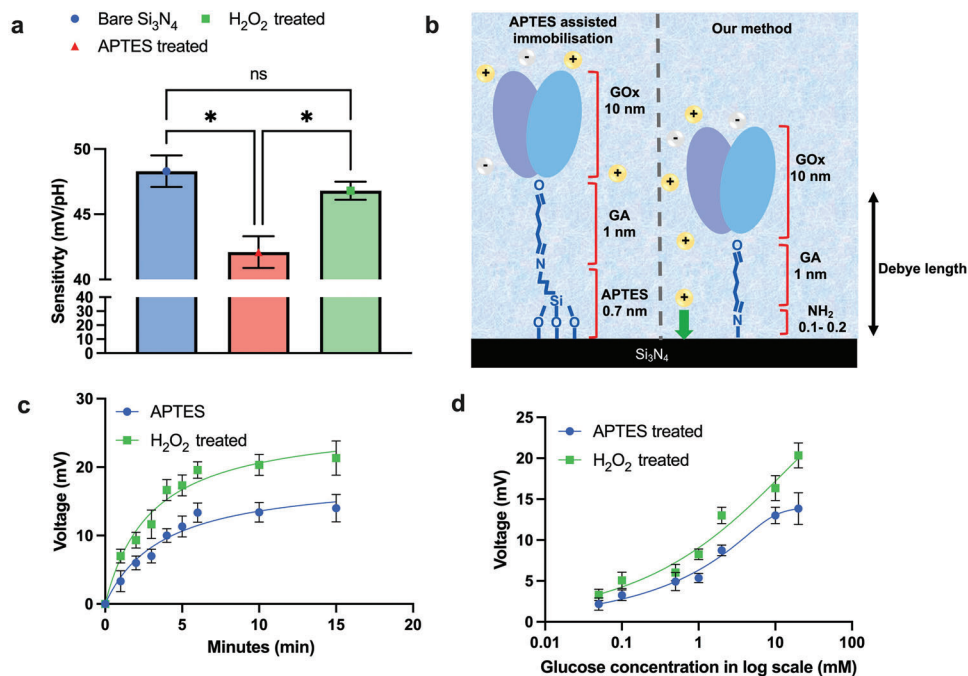


Figure 6. Glucose sensing: a) shows pH sensitivity of $Si_3N_4/SiO_2/Si$ structure. The '*' symbol indicates 'significant' difference and 'ns' denotes 'not significant' difference between the compared columns using Tukey's multiple comparison test with alpha = 0.05. Number of replicates, $n = 3$; b) shows a schematic showing how close biomolecules can be attached using H_2O_2 surface treatment. Essentially, the glucose oxidase (GOx) attached with the linker glutaraldehyde (GA) in APTES assisted immobilization is 1.7 nm away from the surface in comparison to 1.1–1.2 nm in our method; c) shows real time detection of 15 mM glucose with glucose oxidase; d) dose-response of the sensor showing changes in depletion voltage of $Si_3N_4/SiO_2/Si$ structure upon exposure of glucose oxidase to different concentrations of glucose.

increased Debye length effect, as indicated by our results discussed in Figures 4 and 5. In Figure 6b, we show that the glucose oxidase (GOx) attached with the linker glutaraldehyde (GA) in APTES assisted immobilization is approximately 1.7 nm away from the surface in comparison to 1.1–1.2 nm expected in our method. We have adopted these values for APTES immobilization from previous studies conducted by Kim et al.^[39] Immobilizing the enzyme closer to the surface implies that the enzyme-substrate interaction will take place much closer to the surface. In the case of reaction of glucose with glucose oxidase (GOx) there is a release of proton, which is detected by the sensor surface in enhanced manner using sensor surfaces treated with H₂O₂ in comparison to APTES treatment. Figure 6c shows real time study of changes in potential of Si₃N₄/SiO₂/Si structure when exposed to 20 mM of glucose. As observed from the Figure 6c, a much faster reaction kinetics are recorded in the reactions conducted using H₂O₂ treated surfaces. It should be noted that this faster reaction kinetics should be considered as a pseudo enhancement in the rate of reaction. This is because many protons released in the reaction that takes place in APTES treated surfaces (compared to H₂O₂ treated surfaces) are masked by the buffer before they reach the sensor surface, due to Debye length effects. In simpler words, we can say that the reaction takes place at its own rate but the sensor generates different signals for different surface treatments due to Debye length effects. Additionally, when the concentration of glucose is changed, higher potential shifts are yielded, see Figure 6d. Specifically a mean value of 20.3 mV compared to 13.8 mV is observed for a concentration of 15 mM of glucose, a 47% increase in the recorded signal. These results indicate that Debye length effects can be addressed to enhance the bio/chemical sensing signal by use of short length biorecognition layers.

3. Conclusion

In summary, the developed H₂O₂ based protein immobilization strategy yields a higher sensor signal upon binding of proteins as compared to commonly used silane chemistry. Using capacitance voltage characterization, we found that the capacitance of the accumulation and inversion layers of an ISFED structure decreases with an increase in frequency. The effect is more pronounced with the use of low PBS concentration, and no changes are observed in the depletion layer when the surface is functionalized. Overall, the capacitance difference between bare and surface-attached antibodies indicate that biomolecules can be attached to the surface via a short linker from H₂O₂ treatment. This reduces the distance between the ions and the sensor surface, resulting in a shorter Debye length and a higher electric charge density, leading to enhanced sensing performance. While we have used this immobilization strategy for ISFED devices, this can be extended to other transducer surfaces to yield highly sensitive biosensors as demonstrated by our glucose sensing studies.

4. Experimental Section

Immobilization using APTES: A sequential nine step process was followed to immobilize proteins with APTES: 1. Immerse the wafer in 5% APTES in acetone for 6 h at room temperature. Make sure that the petri

dish in which experiment was performed was sealed with paraffin; 2. Rinse the substrate with acetone and DI water; 3. Cure the substrate for 5 min on a hot plate at 90 °C; 4. Immerse the substrate in a solution of glutaraldehyde, GA, (15% in DI) for 3 h; 5. Rinse the substrate thoroughly with DI water or the buffer in which the protein (to be immobilized) solution is made; 6. Dispense the protein solution onto the sample; 7. Rinse the unreacted protein with PBS; 8. Block the unreacted aldehyde groups in 0.2 M ethanolamine for 30 min and 9. Rinse thoroughly with DI water and store in Tris or PBS for further complex reaction. Note that all chemicals used in this process were purchased from Sigma–Aldrich.

Immobilization using GOPTS: To immobilize the proteins with GOPTS following steps were performed: 1. Immerse the cleaned substrate in a GOPTS aqueous solution (98% in aqueous solution) for 45 min. 98% GOPTS in aqueous solution is most stable for protein immobilization; 2. Remove the silanized substrate and dry with nitrogen gas; 3. Cure the substrate for 5 min on a hot plate at 90 °C; 4. Add protein solution and incubate for 6 h or overnight at room temperature; 5. Rinse the protein-coated substrate with the same buffer in which the proteins were suspended; 6. Add 20% ethanol in aqueous solution to block any unreacted GOPTS sites; 7. Rinse thoroughly with DI water and store in Tris or PBS for further complex reaction. All chemicals used in this process were purchased from Sigma–Aldrich.

Immobilization using H₂O₂: Following nine step process was followed to immobilize proteins with H₂O₂: 1. Immerse Si₃N₄ substrate in H₂O₂ (8.25% in aqueous solution) for 3 h; 2. Rinse the substrate thoroughly with DI water; 3. Dry the substrate with nitrogen gas; 4. Immerse the substrate in a solution of glutaraldehyde (15% in DI) for 3 h; 5. Rinse the substrate thoroughly with DI water or the buffer in which the protein (to be immobilized) solution is made; 6. Dispense the protein solution onto the sample; 7. Rinse the unreacted protein with PBS; 8. Block the unreacted aldehyde group in 0.2 M ethanolamine for 30 min; 9. Rinse thoroughly with DI water and store in Tris or PBS for further complex reaction. Note that all reagents used in this process were purchased from Sigma–Aldrich.

TMB Assay: Anti-protein A (antibody for protein A) was used to validate protein immobilization using TMB (3,3',5,5'-tetramethylbenzidine) assay. The samples were incubated with 0.25 mg ml⁻¹ of antibody linked with horseradish peroxidase (HRP) and then washed with PBS. 200 µl of TMB, T-4444 (3,3',5,5'-tetramethylbenzidine) solution was dispensed on the Si₃N₄ surface and the samples were incubated at room temperature for 20 min until a distinct and stabilized color change (usually blue at λ_{max} = 370 and 652 nm) was observed. If the reaction progresses quickly and the color change did not stabilize after 10 min, it can be stopped by adding 50 µl of 2 M sulphuric acid. Absorbance should then be measured at 450 nm. A low-volume spectrophotometer was used (Genova Nano, Jenway Biotech, USA) to detect color changes caused by horseradish peroxidase (HRP) activity. All reagents used in assay were purchased from Sigma–Aldrich.

Glucose Sensing: The oxidation of glucose with glucose oxidase was performed using 8.5 units of oxidase enzyme. The enzyme was immobilized on the surface of the sensor using APTES and H₂O₂ treatment. The surface was then exposed to 0.05, 0.10, 0.50, 1, 2, 10, and 20 mM of glucose concentrations. 15 min of incubation time was allowed before recorded the final sensor reading. Both glucose oxidase and glucose were purchased from Sigma–Aldrich.

Device Fabrication and Capacitance-Voltage Characterization: A conventional electrolyte-insulator-semiconductor (EIS) structure was fabricated with insulator stacks of silicon nitride (Si₃N₄) and silicon oxide (SiO₂) on the P-type silicon wafer with a resistivity of 1–10 Ω-cm. The SiO₂ and Si₃N₄ layer with thickness of 30 nm was grown by thermal oxidation and low-pressure chemical vapor deposition (LPCVD), respectively. To have the bottom electrode of EIS structure, the back-side Si₃N₄ and SiO₂ layer was removed by reactive ion etching with CF₄ gas and buffer oxide etchant, respectively. Then, an aluminum layer with thickness of 300 nm was deposited on back side of Si wafer. These fabricated samples were used to treated in a H₂O₂ and conventional 3-aminopropyltriethoxysilane (APTES) with 4% in volume ratio immersion for 1 h were performed to Si₃N₄ surface. Then, glutaraldehyde (GA) with 1% in volume ratio and alpha-synuclein antibody immobilization with concentration of 40 mg ml⁻¹.

Before and after surface treatments, fourier-transform infrared spectroscopy (FTIR) (Tensor 27, Bruker, Germany) and contact angle measurements (FTA-1000B, First Ten Angstroms, U.S.) were performed to evaluate the difference.

To measure capacitance–voltage (C–V) characteristics of EIS structures in a fixed area, a container made up of polydimethyl-siloxane (PDMS) (Sylgard184A and 184B, Sil-More Industrial Ltd., U.S.) with a self-designed molder with an area of 9x9 mm² was attached on the Si₃N₄ surface by means of O₂ plasma treatment. This container was used to immerse the standard Ag/AgCl reference electrode and background solution including 1X, 0.1X, and 0.01X PBS solution. Then, reference electrode and bottom electrode was connected to the high precision LCR meter (Agilent E4980A, Keysight Technologies, U.S.) for the gate bias and ground bias, respectively. To study the surface modification and debye length effect of EIS structure, two different surface treatments including H₂O₂ and APTES were studied. Frequency from 100 Hz to 200 kHz of the alternating current (AC) trigger signal with a peak-to-peak voltage (Vpp) of 50 mV was applied to measure the C–V curves.

Statistical Analysis: The statistical analysis was either conducted using ANOVA Šídák's multiple comparisons test and the Tukey test multiple comparison test. These tests were conducted using in-built models in GraphPad Prism nine software. Details of these test were explained either in figure captions or/and in the discussion text.

Acknowledgements

The authors would like to thank support from Royal Society, grant number IEC\R3\193004, International Exchanges Cost Sharing Programme.

Conflict of Interest

The authors declare no conflict of interest.

Data Availability Statement

The data that support the findings of this study are available from the corresponding author upon reasonable request.

Keywords

amines, biosensors, debye-length, field-effect transistor, proteins

Received: February 17, 2023

Revised: May 8, 2023

Published online:

- [1] S. Liebana, G. A. Drago, *Essays Biochem.* **2016**, *60*, 59.
- [2] H. Altug, S.-H. Oh, S. A. Maier, J. Homola, *Nat. Nanotechnol.* **2022**, *17*, 5.
- [3] K.-M. Lei, P.-I. Mak, M.-K. Law, R. P. Martins, *Lab Chip* **2016**, *16*, 3664.
- [4] A. Sassolas, L. J. Blum, B. D. Leca-Bouvier, *Biotechnol. Adv.* **2012**, *30*, 489.
- [5] S. Lv, K. Zhang, Y. Zeng, D. Tang, *Anal. Chem.* **2018**, *90*, 7086.
- [6] Z. Qiu, J. Shu, D. Tang, *Anal. Chem.* **2017**, *89*, 5152.
- [7] Y. Lin, Q. Zhou, Y. Lin, D. Tang, R. Niessner, D. Knopp, *Anal. Chem.* **2015**, *87*, 8531.
- [8] S. Lv, K. Zhang, L. Zhu, D. Tang, R. Niessner, D. Knopp, *Anal. Chem.* **2019**, *91*, 12055.

- [9] J. Y. Oh, H.-J. Jang, W.-J. Cho, M. S. Islam, *Sens. Actuators B: Chem.* **2012**, *171*, 238.
- [10] Y. Chen, G. Song, Z. Dong, X. Yi, Y. Chao, C. Liang, K. Yang, L. Cheng, Z. Liu, *Small* **2017**, *13*, 1602869.
- [11] N. Bhalla, M. D. Lorenzo, G. Pula, P. Estrela, *Biosens. Bioelectron.* **2014**, *54*, 109.
- [12] D. Lee, W. H. Jung, S. Lee, E.-S. Yu, T. Lee, J. H. Kim, H. S. Song, K. H. Lee, S. Lee, S.-K. Han, et al., *Nat. Commun.* **2021**, *12*, 1.
- [13] N. Nakatsuka, K.-A. Yang, J. M. Abendroth, K. M. Cheung, X. Xu, H. Yang, C. Zhao, B. Zhu, Y. S. Rim, Y. Yang, *Science* **2018**, *362*, 319.
- [14] M. T. Hwang, M. Heiraniyan, Y. Kim, S. You, J. Leem, A. Taqieddin, V. Faramarzi, Y. Jing, I. Park, A. M. van der Zande, S. Nam, N. R. Aluru, R. Bashir, *Nat. Commun.* **2020**, *11*, 1.
- [15] V. Kesler, B. Murmann, H. T. Soh, *ACS Nano* **2020**, *14*, 16194.
- [16] A. Vacic, J. M. Criscione, N. K. Rajan, E. Stern, T. M. Fahmy, M. A. Reed, *J. Am. Chem. Soc.* **2011**, *133*, 13886.
- [17] N. Nakatsuka, K.-A. Yang, J. M. Abendroth, K. M. Cheung, X. Xu, H. Yang, C. Zhao, B. Zhu, Y. S. Rim, Y. Yang, *Science* **2018**, *362*, 319.
- [18] Q. Xu, Z. Zhang, X. Song, S. Yuan, Z. Qiu, H. Xu, B. Cao, *Sens. Actuators B: Chem.* **2017**, *245*, 375.
- [19] M.-J. Spijkman, J. J. Brondijk, T. C. Geuns, E. C. Smits, T. Cramer, F. Zerbetto, P. Stoliar, F. Biscarini, P. W. Blom, D. M. de Leeuw, *Adv. Funct. Mater.* **2010**, *20*, 898.
- [20] A. Ganguli, V. Faramarzi, A. Mostafa, M. T. Hwang, S. You, R. Bashir, *Adv. Funct. Mater.* **2020**, *30*, 2001031.
- [21] V. Kamysbayev, V. Srivastava, N. B. Ludwig, O. J. Borkiewicz, H. Zhang, J. Ilavsky, B. Lee, K. W. Chapman, S. Vaikuntanathan, D. V. Talapin, *ACS Nano* **2019**, *13*, 5760.
- [22] B. Tashbayev, T. P. Utheim, O. A. Utheim, S. Ræder, J. L. Jensen, M. Yazdani, N. Lagali, V. Vitelli, D. A. Dartt, X. Chen, *Sci. Rep.* **2020**, *10*, 1.
- [23] D. M. Stanbury, *Dalton Trans.* **2022**, *51*, 2135.
- [24] X. Cai, E. E. Tanner, C. Lin, K. Ngamchuea, J. S. Foord, R. G. Compton, *Phys. Chem. Chem. Phys.* **2018**, *20*, 1608.
- [25] D. M. Freire, D. Beeri, K. Pota, H. M. Johnston, P. Palacios, B. S. Pierce, B. D. Sherman, K. N. Green, *Inorg. Chem. Front.* **2020**, *7*, 1573.
- [26] C. J. D. Bakker, N. A. S. John, G. A. George, *Polymer* **1993**, *34*, 716.
- [27] J. D. Merline, C. R. Nair, K. N. Ninan, *J. Macromol. Sci., Part A: Pure Appl. Chem.* **2008**, *45*, 312.
- [28] S. Mezzasalma, D. Baldovino, *J. Colloid Interface Sci.* **1996**, *180*, 413.
- [29] C.-H. Chu, I. Sarangadharan, A. Regmi, Y.-W. Chen, C.-P. Hsu, W.-H. Chang, G.-Y. Lee, J.-I. Chyi, C.-C. Chen, S.-C. Shiesh, et al., *Sci. Rep.* **2017**, *7*, 1.
- [30] N. Nakatsuka, K.-A. Yang, J. M. Abendroth, K. M. Cheung, X. Xu, H. Yang, C. Zhao, B. Zhu, Y. S. Rim, Y. Yang, *Science* **2018**, *362*, 319.
- [31] M. Hinnemo, A. Makaraviciute, P. Ahlberg, J. Olsson, Z. Zhang, S.-L. Zhang, Z.-B. Zhang, *IEEE Sens. J.* **2018**, *18*, 6497.
- [32] B. Li, P. Liu, Z. Xu, S. Zhou, *Nonlinearity* **2013**, *26*, 2899.
- [33] N. Bhalla, D. Lee, S. Sathish, A. Q. Shen, *Nanoscale* **2017**, *9*, 547.
- [34] N. Bhalla, M. D. Lorenzo, G. Pula, P. Estrela, *Biosens. Bioelectron.* **2014**, *54*, 109.
- [35] A. Poghosian, D. T. Mai, Y. Mourzina, M. J. Schöning, *Sens. Actuators B: Chem.* **2004**, *103*, 423.
- [36] E. C. Garnett, Y.-C. Tseng, D. R. Khanal, J. Wu, J. Bokor, P. Yang, *Nat. Nanotechnol.* **2009**, *4*, 311.
- [37] A. S. Dukhin, P. J. Goetz, *Characterization of liquids, dispersions, emulsions, and porous materials using ultrasound*, Elsevier, Amsterdam, Netherlands **2017**.
- [38] G. Liu, S. M. Ciborowski, C. R. Pitts, J. D. Graham, A. M. Buytendyk, T. Lectka, K. H. Bowen, *Phys. Chem. Chem. Phys.* **2019**, *21*, 18310.
- [39] H. Kim, Y. S. Rim, J.-Y. Kwon, *IEEE Sens. J.* **2020**, *20*, 9004.